

Numerical model of a ground-based adaptive telescope. Analysis of image distortions

N.A. Makenova, F.Yu. Kanev, and V.P. Lukin

*Institute of Atmospheric Optics,
Siberian Branch of the Russian Academy of Sciences, Tomsk*

Received October 5, 2005

We present a numerical model of a ground-based telescope, whose optical system incorporates an adaptive system of compensation for image distortions. The model allows us to take into account two distorting factors: misphasing of the telescope's segmented primary mirror and the atmospheric turbulence.

1. Plane-wave model

To study correction for distortions in the adaptive-optics telescope, one needs to simulate propagation of radiation from an extraterrestrial source (an astronomic object), i.e., to develop a plane-wave model. With respect to a numerical experiment, construction of such a model implies simulation of an object that would possess the properties of a plane wave, i.e. the wave whose amplitude and phase in free space are constant in the planes specified by the equation

$$\mathbf{r}\mathbf{k} = \text{const.} \tag{1}$$

Here \mathbf{r} is the radius-vector of a point in the plane; \mathbf{k} is the wave vector.¹

As was shown in solving the problem of wave propagation in vacuum (see Fig. 1) the central part of a Gaussian beam exhibits just these properties. It is seen from this figure that the amplitude and phase in the beam center practically do not differ from those in a plane wave.

A disadvantage of this approach is a low (as compared with the rest of the computational grid) diameter of the part, where a Gaussian beam can be considered a plane wave. For example, on a 256×256 point grid, the size of the area, where the beam amplitude variation does not exceed 3%, is 12×12 points. With such parameters, it is hardly possible to simulate turbulent distortions and estimate anisoplanatism² of the propagation paths.

A "planer" distribution of the amplitude is characteristic of a super Gaussian beam. However, because of the diffraction, a super Gaussian beam undergoes significant changes, and the size of its "plane" part becomes smaller, so the passage to this radiation type does not allow one to considerably increase the size of the computational grid.

For further investigations, we propose that a model of a super Gaussian beam is used as a substitute of a plane wave, which propagates under conditions, when diffraction of the beam as a whole is excluded, while the diffraction on the

inhomogeneities of the refractive index of the medium is taken into account.

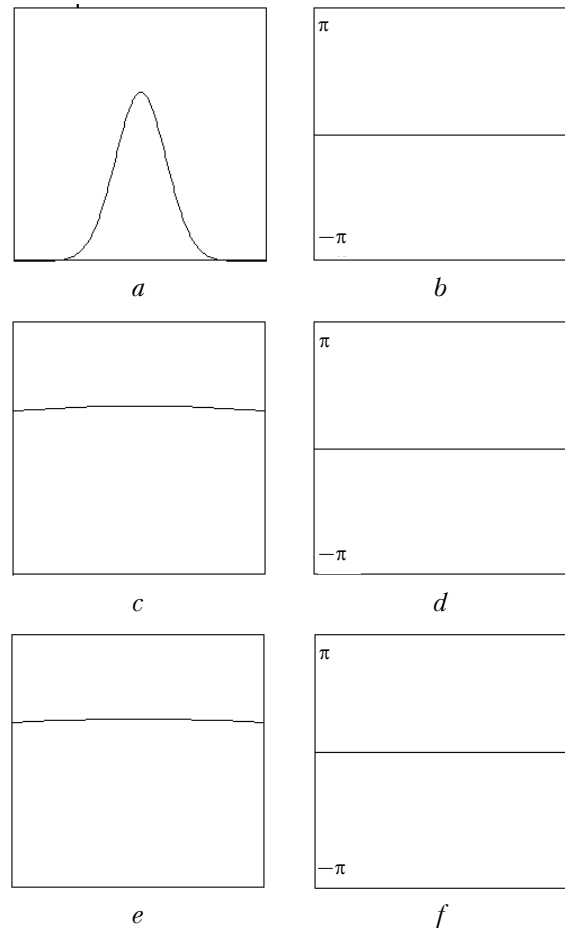


Fig. 1. A plane wave simulated as the central part of the Gaussian beam: initial ($z = 0$) distribution of the amplitude and phase of the beam (cross section) on a 256×256 grid (*a, b*); initial ($z = 0$) distribution of the amplitude in the central part of the beam, a 12×12 grid (*c, d*); distribution of the amplitude and the phase (the central part) of the beam that has traveled a distance of half a diffraction length, a 12×12 grid (*e, f*).

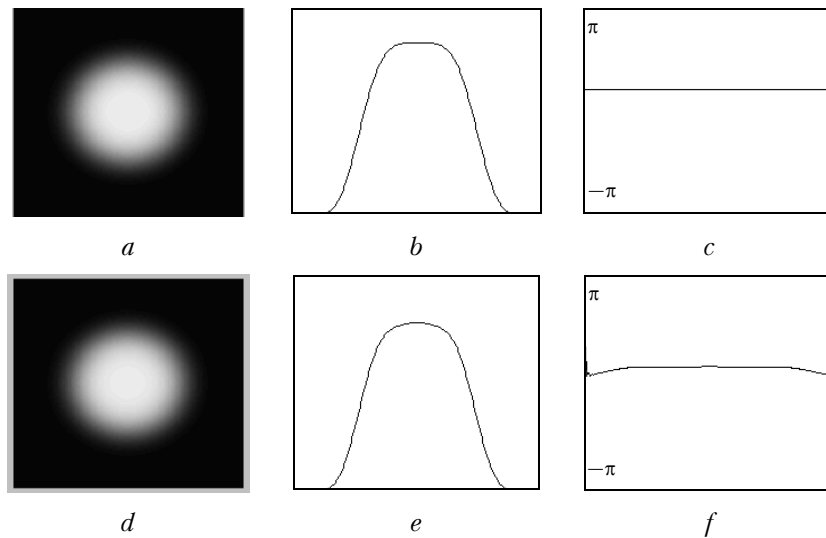


Fig. 2. Diffraction-free propagation of a super Gaussian beam in vacuum: initial ($z = 0$) distribution of the amplitude (a , b) and the phase (c); distribution of the amplitude (d , e), and the phase of the beam (f) after its propagation.

If a medium is non-distorting and the absorption does not have a marked effect, then this model provides for equal distributions of the amplitude in the plane $z = 0$ and in any other plane irrespective of the distance to the source aperture. An example of beam propagation at eliminated diffraction is shown in Fig. 2.

To eliminate diffraction, we placed a set of closely spaced focusing lenses along the propagation path (Fig. 3).

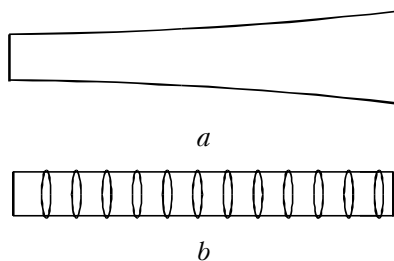


Fig. 3. Schematic representation of the beam propagation under conditions of free diffraction (a) and at an eliminated diffraction (b).

The focal length of each of the lenses was calculated so that the diffraction broadening could be fully compensated for.

Regardless that free diffraction is eliminated, any other phase perturbations will still influence the beam. For example, if in the initial wave front distribution we artificially introduce a singular point, it will cause changes in the amplitude and phase profiles. Atmospheric turbulence also induces changes in both the radiation amplitude and phase (Fig. 4).

The computational grid, where the beam was considered a plane wave, was 80×80 points, and the total grid together with the buffer space was 256×256 points. The radiation passed only through

one phase screen. The initial distribution of the field amplitude was uniform. At the distance $z > 0$ behind the phase screen (the screen was positioned in the plane $z = 0$, Fig. 4c) we observed modulation of the amplitude distribution (Fig. 4b).

The phase profile of the wave reflects (since diffraction caused by inhomogeneities is still assumed to occur) variations of the refractive index in the screen. The phase distribution is shown in Fig. 4d.

As is demonstrated by numerical experiments, for small (compared to diffraction length) paths these properties are characteristic of the central part of a Gaussian beam as well. The main difference with the above plane wave model is that solution of the problem that involves a beam requires a much larger buffer zone.

2. The model of a ground-based telescope. Account of the distorting factors

The plane-wave model developed has allowed us to easily construct an ideal (i.e., neglecting the restrictions imposed by a wave-front sensor and an adaptive mirror) model of a ground-based telescope. The calculation scheme of the numerical experiment performed with the use of the model is shown in Fig. 5, wherefrom we see that the plane wave generated by an extraterrestrial source is incident on the layer of distorting medium and, having passed through it, the radiation undergoes the amplitude and phase modulation. Then the light flux is focused with the primary mirror. Turbulent disturbances of the refractive index cause distortions of the image constructed in the focal plane. The distortions are compensated for by phase control of the radiation wave front.

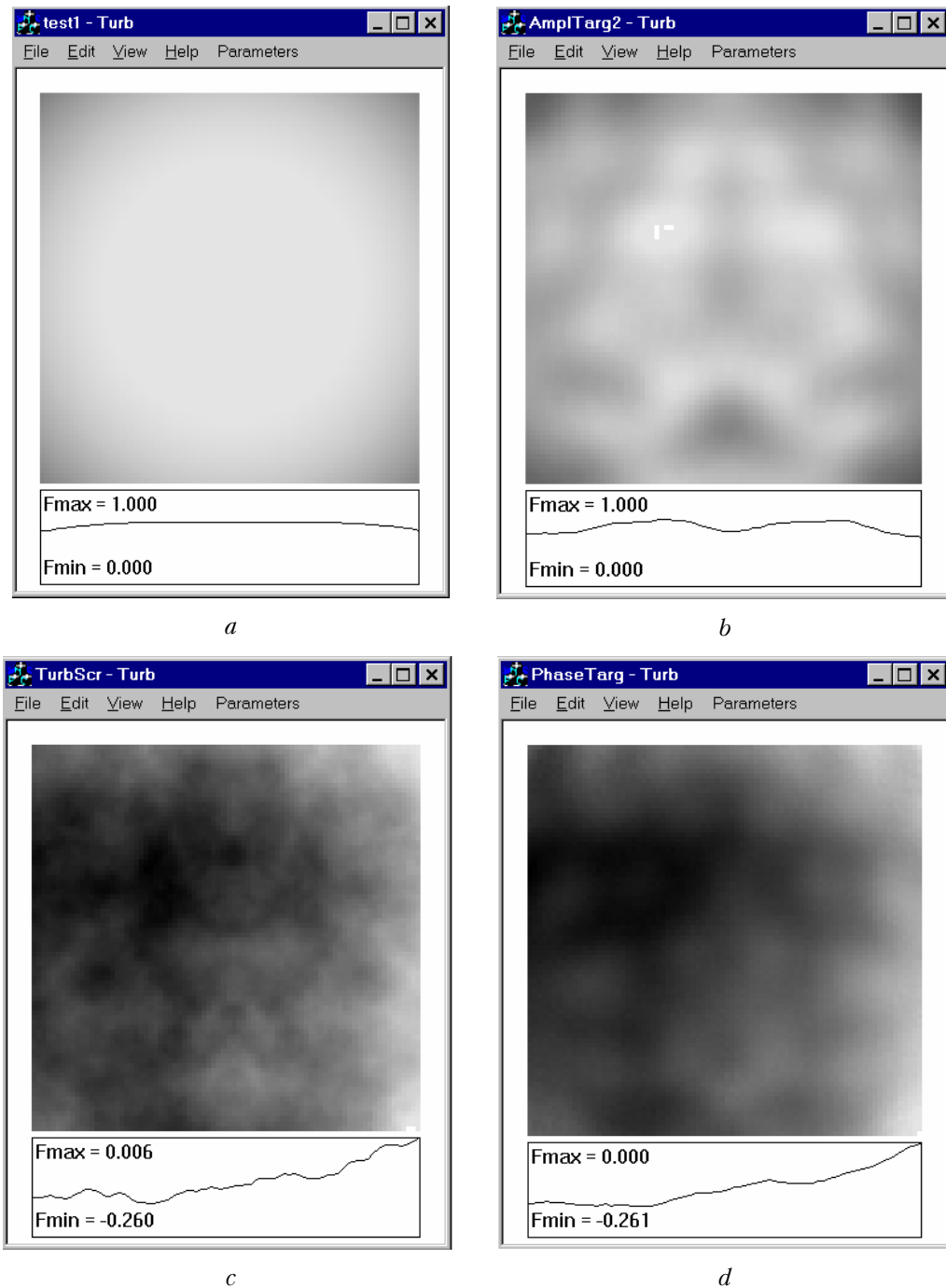


Fig. 4. Propagation of the plane wave in a turbulent medium: initial distribution of the amplitude (*a*); distribution of the amplitude after propagation through the medium (*b*); turbulent changes of the refractive index (*c*); wave phase after propagation (*d*).

Now let us list some other applications of the model. With a few modifications done it allows one to analyze the effect of anisoplanatism of the radiation arrival angle from the source and the reference wave; to estimate the resolution needed for discerning binary stars depending on the intensity of turbulent distortions; to develop the methods that would allow allocation of a low-intensity source near a bright object to be done. Another class of problems

involves the effect of the elements of adaptive system on the imaging quality. For their solution we can use the models of the Hartmann sensor and an elastic deformable mirror.^{3,4}

Now consider briefly one more source of distortions in the telescope, namely, random displacements of the segments of the primary mirror. Loss of quality of the image due to misphasing is demonstrated in Fig. 6, which shows the cross

sections of focused radiation at different variances of random displacements of the segments. These distributions are normalized to the diffraction-limited

intensity. In Fig. 6, we can see lowering of the height of the principal maximum and appearance of additional maxima.

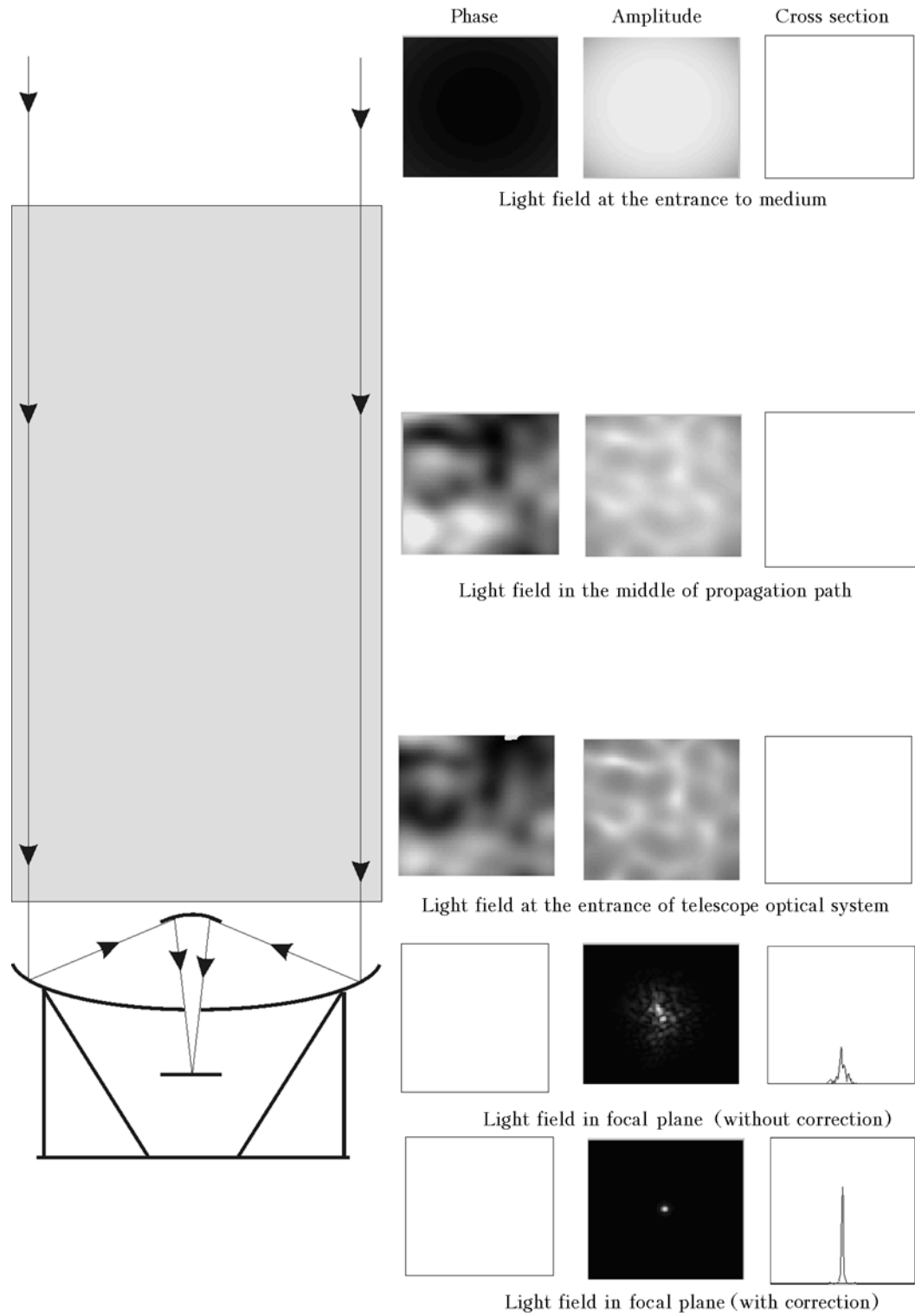


Fig. 5. The model of the adaptive telescope.

The corresponding reduction of the Strehl ratio is illustrated in Fig. 7, from which we can compare the results obtained in the numerical experiment with the theoretical ones. R. Tyson in his monograph⁵ says that to estimate distortions, we can use the formula, according to which the Strehl ratio is exponentially dependent on the variance:

$$St = \exp(-\sigma^2).$$

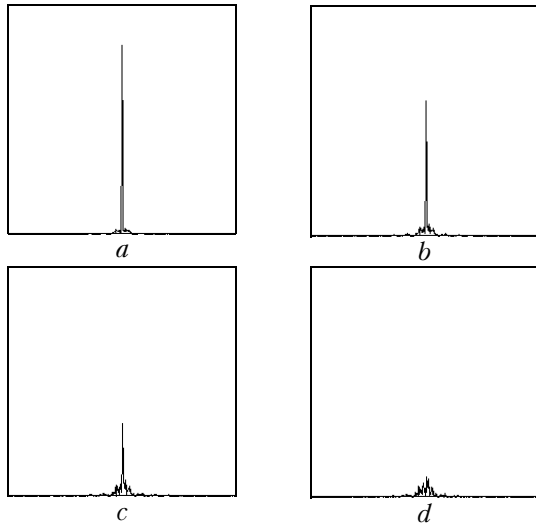


Fig. 6. The cross section of the focused radiation spot in the telescope at the distribution normalized to the value of diffraction-limited intensity. The variance of random displacements equals $\lambda/4$ (a), $\lambda/2$ (b), $3\lambda/4$ (c), and λ (d).

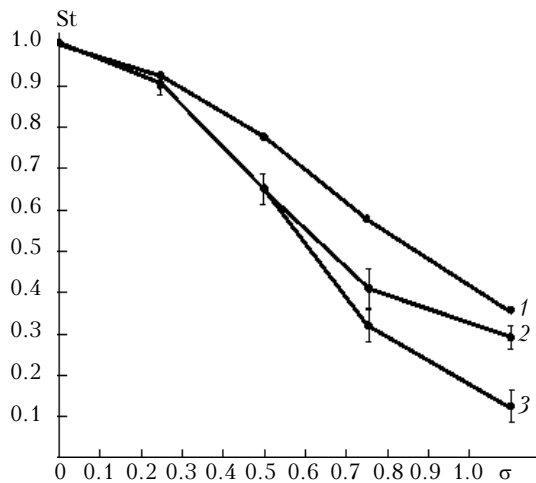


Fig. 7. The Strehl ratio as a function of random shifts variance normalized to the radiation wavelength: theoretical results (curve 1); results of the numerical experiment with a mirror having 32×32 segments (curve 2) and 8×8 (curve 3).

In Fig. 7, this dependence corresponds to curve 1. Our simulation shows that with the increase of the displacement amplitude in the telescope the criterion decreases much faster (curves 2 and 3, Fig. 7).

However, the displacements of the segments result not only in a decrease of the St criterion.

Without normalization, one can see, in the intensity distributions, a periodic structure with a pronounced central peak and secondary maxima (Fig. 8).

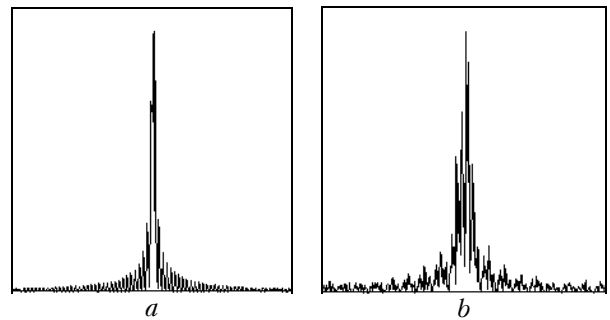


Fig. 8. Structure of the image (without normalization): the mirror of 8×8 segments and the variance of the random displacements equals λ (a); 32×32 segments and the variance equals λ (b).

The distortions caused by random tilts of the segments have similar character. The way they manifest themselves is illustrated in Fig. 9.

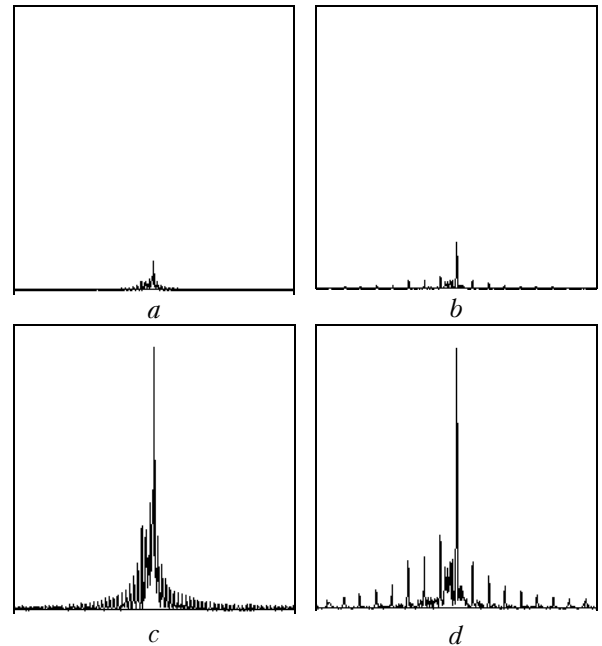


Fig. 9. Cross section of the image in the telescope at random tilts of segments. Phase shift within one segment equals one wavelength. The numerical model included an 8×8 -segment mirror, normalization of the distribution is performed to the diffraction-limited intensity value (a) as well as the distribution without normalization (c). For the 32×32 -segment mirror, a normalized distribution (b) and distribution without normalization (d) have also been calculated.

Like in the above case, misphasing in the mirror leads to losses in intensity and to appearance of secondary maxima.

Somewhat different is the character of distortions for the mirror with a larger number of segments (32×32 , Figs. 9b and d). In this case, the above periodic structure undergoes changes in the intensity that has a larger period and higher maxima.

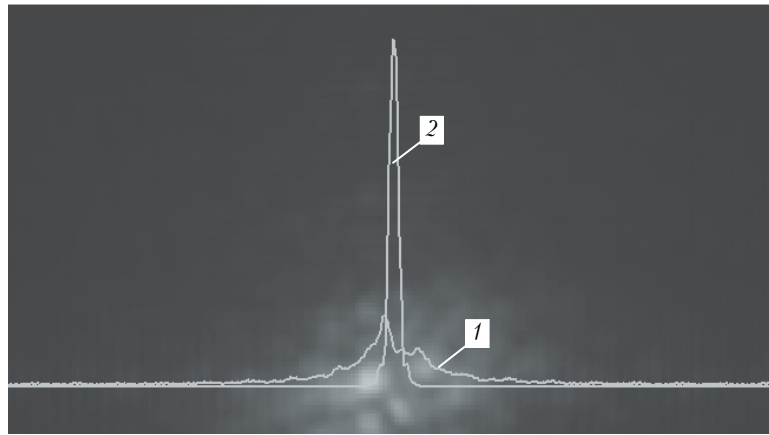


Fig. 10. Mutual influence of distortions (turbulence and misphasing; turbulent distortions are averaged over 50 realizations). Cross section of the focused radiation (curve 1); diffraction-limited distribution (curve 2).

Overall, we may conclude that random displacements and tilts of the segments lead to strong image distortions. In particular, for the displacements with the variance comparable to one wavelength, the Strehl criterion decreases by five times and lower as compared with the diffraction-limited value.

The effect of turbulence and misphasing on the distribution of the focused radiation is illustrated in Fig. 10. As is seen, the above periodic structure is smeared and it is now hardly possible to discriminate between the contributions of separate distortion sources.

3. Phasing of a segmented mirror

A segmented mirror is usually phased using mechanical (capacitance- or inductive-type) sensors of segment displacements^{6,7} in combination with the optical methods. We propose to abandon sensors via extending of the operation range of purely optical methods (so, to apply only optical methods). Thus the phasing algorithm is simplified and, perhaps, becomes more cheap.

Reduction of the segment displacement can be performed through the procedure of searching for the functional extreme, which is set by the expression

$$J_{\text{cor}}(z) = \frac{\sum A_1(x, y)A_2(x, y)}{\sum A_1(x, y)A_1(x, y)}. \quad (2)$$

This parameter shows to what extent the interferogram obtained at reflection of a laser beam from the neighboring segments differs from the interferogram observed at a zero displacement (thus, the value of the ratio is determined with the use of the reference interferogram obtained at a zero relative displacement). In Eq. (2), $A_1(x, y)$ stands for the distribution of the optical field intensity in the reference interferogram, and $A_2(x, y)$ is the intensity distribution for the interferogram of the mirror with displaced segments. At the exactly matched interferograms, $J_{\text{cor}}(z) = 1$ and starts decreasing with

the increase of the differences between the two patterns.

In the numerical experiments performed, we have shown that the phasing accuracy is determined by the initial displacement Δz : at $\Delta z < \lambda/2$, the mirror surface obtained via arrangement of segments is flat, and at $\Delta z > \lambda/2$ the algorithm gives the increase in the relative displacement. Changes in the relative segment displacement for both of the cases are shown in Fig. 11.

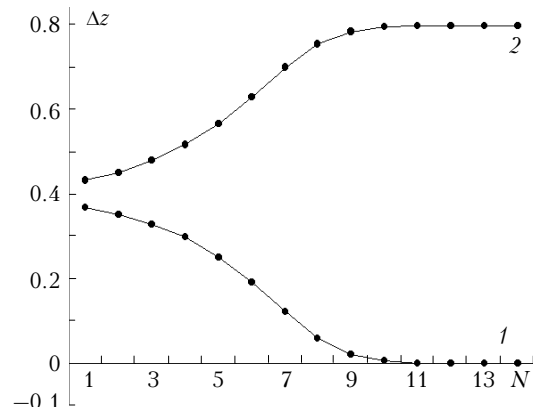


Fig. 11. Changes in the relative displacement of the mirror segments Δz during the aperture sensing (the wavelength $\lambda = 0.8 \mu\text{m}$). N is the iterative step number. $\Delta z = 0.367 \mu\text{m}$ (curve 1), $\Delta z = 0.433 \mu\text{m}$ (curve 2).

Extension of the tolerance range of the initial displacements is possible with introduction of an additional wavelength to the control algorithm. The values of the ratio J_{cor} specified in Eq. (2) and calculated at a change with respect to the segment displacement (scanning) for the wavelengths $\lambda = 0.6$ and $0.8 \mu\text{m}$ are shown in Fig. 12.

This diagram shows that the physically equal displacements of segments gives different phase shifts for different wavelengths, that is why the ratio maxima coincide only at $\Delta z = 0$ and $2.4 (-2.4) \mu\text{m}$. Note that 2.4 is the smallest number that can be

divided by 0.6 and 0.8 without a remainder. In this case, phase shifts will be 8π and 6π , respectively. Therefore, introduction, into the algorithm, of the requirement that the control stops only after the maximum of the ratio has been found at the two wavelengths, allows us to increase the dynamic range of compensation for the random displacements.

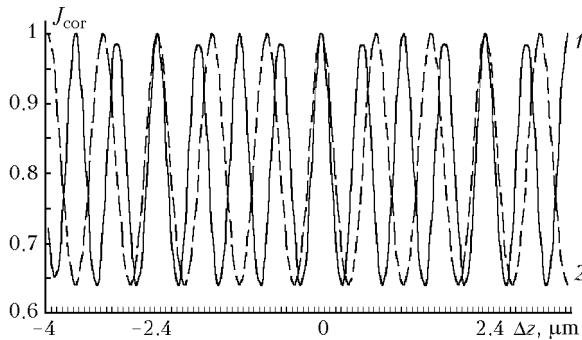


Fig. 12. Dependences of the ratio J_{cor} on the relative displacement of mirror segments Δz : $\lambda = 0.6 \mu\text{m}$ (curve 1), $\lambda = 0.8 \mu\text{m}$ (curve 2).

A further extension of the range is obtained via proper choice of the wavelengths of interfering beams and by introducing third wavelength. The data on the intervals of tolerable deviations are given in Table 1.

Table 1. The maximum displacement Δz , at which mirror phasing is possible; λ_i are the wavelengths at which the control is performed

$\lambda_1, \mu\text{m}$	$\lambda_2, \mu\text{m}$	$\lambda_3, \mu\text{m}$	$\Delta z, \mu\text{m}$
0.8	—	—	0.36
0.6	—	—	0.26
0.6	0.8	—	2.34
0.7	0.8	—	5.55
0.6	0.7	0.8	33.4

The results given in Table 1 allow us to conclude that the method described in this paper makes it possible to greatly increase the range of the optical methods of phasing.

References

1. M. Born and E. Wolf, *The Principles of Optics* (Pergamon Press, Oxford—London—Edinburgh—New York—Paris—Frankfurt, 1964)
2. B.M. Welsh and C.S. Gardner, *J. Opt. Soc. Am. A* **8**, No. 1, 69–80 (1991).
3. F.Yu. Kanev, V.P. Lukin, and N.A. Makenova, *Proc. SPIE* **5026**, 190–197 (2002).
4. F.Yu. Kanev, V.P. Lukin, and B.V. Fortes, *Atmos. Oceanic Opt.* **5**, No. 12, 852–854 (1992).
5. R.K. Tyson, *Principles of Adaptive Optics* (Academic Press, San Diego, 1991), 233 pp.
6. N. Yaitskova, K. Dohlen, and Ph. Dierickx, *J. Opt. Soc. Am. A* **20**, No. 8, 1563–1574 (2003).
7. W. Zou, *J. Opt. Soc. Am. A* **18**, No. 3, 638–649 (2001).